PHYSICAL REVIEW B **96**, 201408(R) (2017)

Calibration of the fine-structure constant of graphene by time-dependent density-functional theory

A. Sindona,[1,2,*] M. Pisarra,[3] C. Vacacela Gomez,[1,4] P. Riccardi,[1,2] G. Falcone,[1,2] and S. Bellucci[5]

[1]*Dipartimento di Fisica, Università della Calabria, Via P. Bucci, Cubo 30C, I-87036 Rende (CS), Italy*

[2]*INFN, sezione LNF, Gruppo collegato di Cosenza, Cubo 31C, I-87036 Rende (CS), Italy*

[3]*Departamento de Química, Universidad Autónoma de Madrid, C/Fco. Tomás y Valiente 7, E-28049 Madrid, Spain*

[4]*Escuela Superior Politécnica de Chimborazo, Panamericana Sur Km 1 1/2, Riobamba EC-060155, Ecuador*

[5]*INFN–Laboratori Nazionali di Frascati (LNF), Via E. Fermi 40, I-00044 Frascati, Italy*

(Received 28 September 2017; published 17 November 2017)

One of the amazing properties of graphene is the ultrarelativistic behavior of its loosely bound electrons, mimicking massless fermions that move with a constant velocity, inversely proportional to a fine-structure constant α_g of the order of unity. The effective interaction between these quasiparticles is, however, better controlled by the coupling parameter $\alpha_g^* = \alpha_g/\epsilon$, which accounts for the dynamic screening due to the complex permittivity ϵ of the many-valence electron system. This concept was introduced in a couple of previous studies [Reed *et al.*, Science **330**, 805 (2010) and Gan *et al.*, Phys. Rev. B **93**, 195150 (2016)], where inelastic x-ray scattering measurements on crystal graphite were converted into an experimentally derived form of α_g^* for graphene, over an energy-momentum region on the eV Å^{-1} scale. Here, an accurate theoretical framework is provided for α_g^*, using time-dependent density-functional theory in the random-phase approximation, with a cutoff in the interaction between excited electrons in graphene, which translates to an effective interlayer interaction in graphite. The predictions of the approach are in excellent agreement with the above-mentioned measurements, suggesting a calibration method to substantially improve the experimental derivation of α_g^*, which tends to a static limiting value of $\sim$0.14. Thus, the *ab initio* calibration procedure outlined demonstrates the accuracy of perturbation expansion treatments for the two-dimensional gas of massless Dirac fermions in graphene, in parallel with quantum electrodynamics.

DOI: 10.1103/PhysRevB.96.201408

Graphene, the two-dimensional (2D) allotrope of carbon with sp^2-bonded honeycomb lattice, is the first discovered [1] and currently most studied atomically thin material [2,3], due to a variety of potential uses [4]. On the electronic side, the unique properties of graphene stem from its semimetallic band structure around the Fermi energy E_F, with the valence (π) and conduction (π^*) energy levels exhibiting a conical dispersion vs the in-plane momentum at the six corners of the (hexagonal) first Brillouin zone (1$^{\text{st}}$BZ), i.e., the Dirac K (or K') points [5]. This peculiar feature has allowed the development of a quasiparticle description of charge transport [6], consisting of charge carriers that behave as massless Dirac fermions on a velocity scale, characterized by the group velocity of the π and π^* electrons at the Dirac points, i.e., the *Fermi velocity* $v_F \sim c/300$, with $c \sim 137$ being the velocity of light in Hartree atomic units (used throughout unless otherwise specified).

Nonetheless, the quasiparticle interaction in this picture depends on a (bare) effective fine-structure constant $\alpha_g = 1/v_F \sim 2.2$ [7–12], being much larger than the vacuum fine-structure constant $\alpha = 1/c$ of quantum electrodynamics (QED). Indeed, many-body corrections to v_F [12–15] can significantly lower α_g, which, however, contrary to QED, remains too large for perturbation treatments. On the other hand, α_g is too small for strong-coupling approaches. Attempts to reduce α_g by changing the supporting dielectric medium lead to $\alpha_g^* = \alpha_g/\epsilon$ [16], where ϵ is the constant permittivity of the "background" that embeds the graphene sheet. Even in this case, α_g^* remains not far from unity.

A more complete "view" of the interaction strength between the band electrons in graphene amounts to replacing $1/\epsilon$ in α_g^* with the dynamic inverse permittivity [17–19], obtained by transferring an energy ω and a momentum $\mathbf{q}$ to the system. On these bases, inelastic x-ray scattering experiments were performed to determine the many-electron screening in crystal graphite [8,10], followed by reconstruction methods to derive the full susceptibility of freestanding graphene and a diagrammatic formalism structured in powers of α_g^*.

Here, it is demonstrated that time-dependent (TD) density-functional theory (DFT) provides a reliable theoretical framework for the above-mentioned measurements, with a key role being played by the bare Coulomb interaction between excited electrons within the graphene sheet [20–25], which reflects in the interlayer interaction in graphite [8,10,26–28]. A substantial improvement on the determination of α_g^* is presented, suitable for transferred energies from the far-infrared to the extreme ultraviolet, and in-plane momenta up to $\sim$1 Å^{-1}. An exploration of the small in-plane momentum region yields the static limiting value $\alpha_g^* \sim 0.14$, in agreement with [8], which supports the idea that the massless Dirac fermions of graphene experience a sufficiently weak interaction. More importantly, a procedure to extrapolate the effective fine-structure constant of Dirac-cone materials is outlined.

To begin, the ground-state properties of graphene were calculated by a standard plane-wave (PW) DFT approach [29], using the local density approximation (LDA) [30] and eliminating the core electrons by a norm-conserving pseudopotential [31]. An energy cutoff of 25 hartree [32] was applied to compute the Kohn-Sham (KS) electron states

*antonello.sindona@fis.unical.it

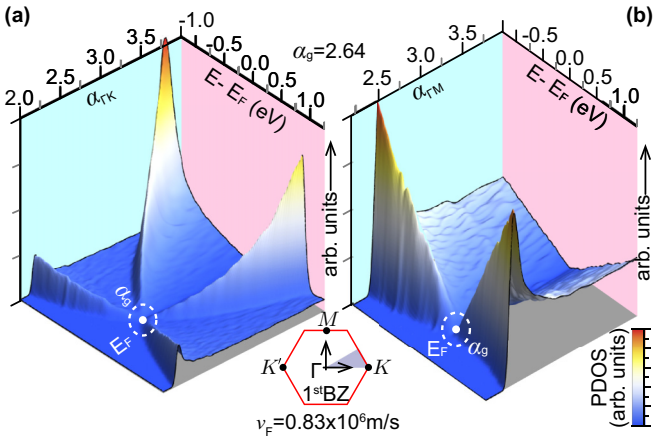

FIG. 1. Static fine-structure constant of graphene extracted from the PDOS vs the π-π^* energy $E - E_F$ and the inverse group velocities $\alpha_{\Gamma K} = 1/v_{\Gamma K}$(a), $\alpha_{\Gamma M} = 1/v_{\Gamma M}$(b).

$|\nu\mathbf{k}\rangle$ and corresponding energies $\varepsilon_{\nu\mathbf{k}}$ [33,34], indexed by their band number ν and wave vector $\mathbf{k}$ in the 1stBZ (inset of Fig. 1). The bulk geometry inherent to PW-DFT was modeled by an infinitely periodic array of elementary graphene cells, with in-plane lattice constant of 2.46 Å, replicated at an out-of-plane distance L of 20 Å. The self-consistent run was performed on the (four) valence and lowest conduction bands with a Monkhorst-Pack grid of 60×60×1 $\mathbf{k}$ points [35], sampling the 1stBZ [32]. Then, the KS structure was refined in three non-self-consistent runs based on (i) 900×900×1 $\mathbf{k}$ points with the same bands as the self-consistent run, (ii) 720×720×1 $\mathbf{k}$ points with the lowest set of eight bands, and (iii) 360×360×1 $\mathbf{k}$ points with the lowest set of sixty bands [Fig. S1(a) of [32]].

The output of dataset (i) was accurate enough to fix the Dirac-cone features of the π and π^* electrons [Fig. S1(b)], such as the Fermi velocity v_F at the K (or K') points, estimated to have a value of 0.83×10^6 m/s (Fig. S2 of [32]), and the static fine-structure constant $\alpha_g = 2.64$ (Fig. 1). It is worth recalling that the anisotropic behavior of the π and π^* bands, for wave vectors distant more than ∼0.01 Å^{-1} from the Dirac points, has been conjectured to suggest the presence of distinct types of charge carriers along different directions of the reciprocal space, which generate markedly different extrinsic plasmon responses at probing energies smaller than 1.0 eV [36]. This point is further clarified here, by looking at the projected (P) density of states (DOS) of the π and π^* states as a function of their energy E, relative to E_F, and the static fine-structure constant. The latter is defined in this context as the inverse group velocity along selected high-symmetry directions of the 1stBZ, namely, $\alpha_{\Gamma K} = 1/v_{\Gamma K}$, along ΓK, and $\alpha_{\Gamma M} = 1/v_{\Gamma M}$, along ΓM. In the $(E - E_F, \alpha_{\Gamma K})$ plane [Fig. 1(a)], the PDOS approaches α_g (zero-DOS point) along two distinct "branches," which define two types of quasimassless Dirac fermions, whose interaction is controlled by different coupling constants, right outside the linear region where the Dirac-cone approximation is violated [see also Fig. S3(a) of [32]]. On the other hand, in the $(E - E_F, \alpha_{\Gamma M})$ plane [Fig. 1(b)], the PDOS approaches α_g following a single branch, which defines a single type of charge carriers and coupling parameter [see also Fig. S3(b) of [32]].

Next, the unperturbed susceptibility of the KS electrons was calculated in response to an energy-momentum transfer $(\omega, \mathbf{q})$ from an incident particle (electron or photon). This quantity is generally represented in reciprocal space as [37,38]

$$\chi^0_{\mathbf{GG}'} = \frac{2}{\Omega} \sum_{\mathbf{k},\nu,\nu'} \frac{(f_{\nu\mathbf{k}} - f_{\nu'\mathbf{k}+\mathbf{q}}) \rho^{\mathbf{kq}}_{\nu\nu'}(\mathbf{G})\, \rho^{\mathbf{kq}}_{\nu\nu'}(\mathbf{G}')^*}{\omega + \varepsilon_{\nu\mathbf{k}} - \varepsilon_{\nu'\mathbf{k}+\mathbf{q}} + i\eta}, \quad (1)$$

where $\mathbf{G}, \mathbf{G}'$ are reciprocal lattice vectors of in-plane components $\mathbf{g}, \mathbf{g}'$ and out-of-plane components G_z, G'_z. The $\chi^0_{\mathbf{GG}'}$ matrix elements, normalized to the electron volume Ω, include a factor of 2 for the electron spin, the Fermi-Dirac occupation numbers $f_{\nu\mathbf{k}}, f_{\nu\mathbf{k}+\mathbf{q}}$, a lifetime broadening parameter η (of the order of 10^{-2} eV), and the density correlation terms $\rho^{\mathbf{kq}}_{\nu\nu'}(\mathbf{G}) = \langle \nu\mathbf{k}|e^{-i(\mathbf{q}+\mathbf{G})\cdot\mathbf{r}}|\nu'\mathbf{k}+\mathbf{q}\rangle$, $\rho^{\mathbf{kq}}_{\nu\nu'}(\mathbf{G}')^* = \langle \nu'\mathbf{k}+\mathbf{q}|e^{i(\mathbf{q}+\mathbf{G}')\cdot\mathbf{r}}|\nu\mathbf{k}\rangle$. The 2D macroscopic average of Eq. (1) is provided by $\chi^M_0 = \chi^0_{\mathbf{00}}$, with $\chi^0_{\mathrm{2D}} = \chi^M_0 L$ being the macroscopic unperturbed susceptibility of graphene in two dimensions.

The KS structure from datasets (ii) and (iii) was plugged into Eq. (1) to explore the lower infrared ($\omega < 1$ eV) and midinfrared to extreme ultraviolet ranges ($\omega < 35$ eV), respectively. Subsequently, the full susceptibility was computed from the central equation of TDDFT [17]

$$\chi_{\mathbf{GG}'} = \chi^0_{\mathbf{GG}'} + (\chi^0 v \chi)_{\mathbf{GG}'}, \quad (2)$$

whose solution provides the macroscopic average $\chi^M = \chi_{\mathbf{00}}$.

Working in the random-phase approximation at room temperature, an in-plane transferred momentum $\mathbf{q}$ was considered and the v operator in Eq. (2) was represented by a Coulomb interaction of matrix elements

$$v_{\mathbf{GG}'}(L) = \frac{2\pi\delta_{\mathbf{gg}'}}{|\mathbf{q}+\mathbf{g}|} \iint_{-L/2}^{L/2} dz\, dz' e^{i(G_z z - G'_z z') - |\mathbf{q}+\mathbf{g}||z+z'|}, \quad (3)$$

truncated at half interslab distance.

The $v_{\mathbf{GG}'}(L)$ terms have been carefully designed to describe the dielectric response of mono- and bilayer graphene, graphene nanoribbon arrays, and freestanding silicene in the whole range of momentum transfers over the 1stBZ [20–25]. Interestingly enough, the leading component $v_{\mathbf{00}}(L) = \frac{4\pi}{q^2} - \frac{4\pi}{Lq^3}(1 - e^{-qL})$ tends to $v_{\mathrm{2D}}L$, where $v_{\mathrm{2D}} = \frac{2\pi}{q}$ is the 2D Coulomb potential, for vanishingly small momenta ($qL \ll 1$ limit), whereas in the opposite case ($qL \gg 1$ limit) it behaves as the three-dimensional (3D) Coulomb potential $\frac{4\pi}{q^2}$. Indeed, the cutoff in $v \to v_{\mathbf{GG}'}(L)$ cancels the residual coupling between the 2D replicas of the bulk DFT approach, which gives a reliable expression for the inverse dielectric matrix $(\epsilon^{-1})_{\mathbf{GG}'} = \delta_{\mathbf{GG}'} + (v\chi)_{\mathbf{GG}'}$ and its macroscopic average $(\epsilon^M)^{-1} = 1 + (v\chi)_{\mathbf{00}}$. The imaginary part of the latter is proportional to the energy loss function $E_{\mathrm{LOSS}} = -\mathrm{Im}[(\epsilon^M)^{-1}]$.

Crystal local-field effects [39] were included in χ^M and ϵ^M by reducing χ to a 61×61 matrix [32], indexed by reciprocal lattice vectors of lengths below 9.5 Å^{-1}. The neglect of crystal local fields turns Eq. (2) into a scalar equation that, in the low-q limit $v_{\mathbf{00}}(L) \to v_{\mathrm{2D}}L$, allows one to define the 2D macroscopic susceptibility $\chi^M_{\mathrm{2D}} = \frac{\chi^0_{\mathrm{2D}}}{1 - v_{\mathrm{2D}}\chi^0_{\mathrm{2D}}}$, permittivity $\epsilon^M_{\mathrm{2D}} = \frac{1}{1 - v_{\mathrm{2D}}\chi^0_{\mathrm{2D}}}$, and loss function $E^{\mathrm{2D}}_{\mathrm{LOSS}} = \mathrm{Im}(v_{\mathrm{2D}}\chi^0_{\mathrm{2D}})$.

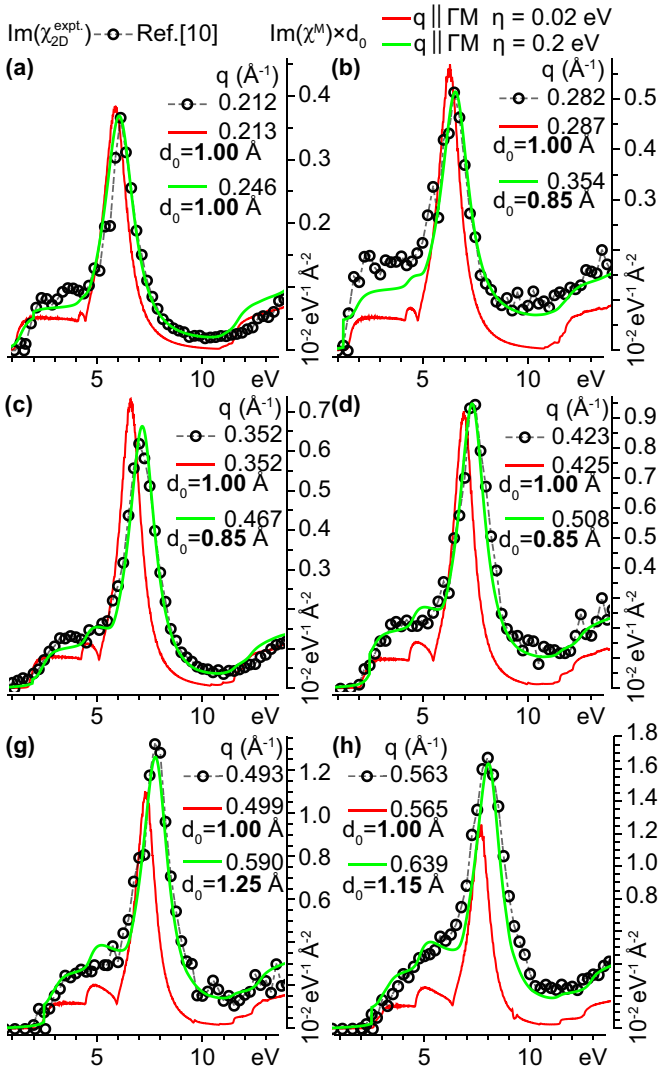

FIG. 2. Experimentally derived susceptibility $\mathrm{Im}(\chi_{2D}^{\mathrm{expt.}})$ of [10] and macroscopic susceptibility $\mathrm{Im}(\chi^{M})$, obtained from Eq. (2) with $v \to v_{\mathbf{GG}'}(L)$ and the KS structure of dataset (iii). $\mathrm{Im}(\chi^{M})$ is multiplied by a typical length d_0 to match the dimensions of $\mathrm{Im}(\chi_{2D}^{\mathrm{expt.}})$. The closest values of $\mathbf{q} \| \Gamma M$ to the measured in-plane momenta are selected to represent $\mathrm{Im}(\chi^{M})$, with a broadening lifetime η of 0.02 eV (red). The $\mathbf{q}$-shifted spectra (green) are broadened by 0.2 eV to match the experimental uncertainties.

Figure 2 (or Fig. S4 of [32]) presents a comparison of the calculated imaginary susceptibility of graphene $\mathrm{Im}(\chi^{M})$ with its experimental counterpart $\mathrm{Im}(\chi_{2D}^{\mathrm{expt.}})$, derived in [8,10]. Theoretical calculations are consistent with the experiments, although the agreement with data is excellent if an increasingly small positive shift in q (with $q \lesssim 0.1$ Å^{-1}) is applied to $\mathrm{Im}(\chi^{M})$. The main reason for this discrepancy is due to the fact that $\mathrm{Im}(\chi_{2D}^{\mathrm{expt.}})$ was obtained from the measured imaginary susceptibility of graphite $\mathrm{Im}(\chi_{3D}^{\mathrm{expt.}})$, using $\chi_{2D}^{\mathrm{expt.}} = \frac{\chi_{3D}^{\mathrm{expt.}} d}{1-(v_{2D}-v_{3D})\chi_{3D}^{\mathrm{expt.}} d}$. Such a conversion works under the following assumptions: the macroscopic unperturbed susceptibility of graphene χ_0^{M} and that of graphite are equal [40]; the electron-electron interaction in graphene is purely two-dimensional $[v \to \delta_{\mathbf{GG}'} v_{2D} L$ in Eq. (2)]; the role of crystal local fields can be neglected, i.e., the full susceptibility of graphene is χ_{2D}^{M}; the interaction of graphene layers in graphite, separated by $d = 3.35$ Å, can be modeled by the interlayer potential $v_{3D} = v_{2D} \frac{\sinh(qd)}{\cosh(qd)-\cos(q_z d)}$ [26,27], with q_z being an out-of-plane momentum. An open boundary version of the interlayer potential, suitable for finite numbers of layers, was introduced in [28]. However, the use of v_{2D} for the electron-electron interaction in graphene is strictly valid for vanishingly small momenta, which are far from the experimental values (in the range of 0.2 to 0.8 Å^{-1}) acquired in [8,10]. Indeed, the macroscopic inverse permittivity $(\epsilon^{M})^{-1}$ appears to accurately predict the π-plasmon loss peaks of graphene measured in [41], significantly improving the results that would be obtained with $(\epsilon_{2D}^{M})^{-1}$. On the other hand, both $(\epsilon^{M})^{-1}$ and $(\epsilon_{2D}^{M})^{-1}$ are in close agreement with electron-energy-loss measurements performed in [42] at $q \lesssim 0.1$ Å^{-1} (see Fig. S5 and discussion in [32]). Another clue in favor of the use of $v_{\mathbf{GG}'}(L)$ in spite of v_{2D} is provided in Figs. 3(a), 3(c), and 3(e), where χ_0^{M} is compared with the macroscopic unperturbed susceptibility of graphene $\chi_0^{\mathrm{expt.}}$, experimentally derived from $\chi_{2D}^{\mathrm{expt.}} = \frac{\chi_0^{\mathrm{expt.}}}{1-v_{2D}\chi_0^{\mathrm{expt.}}}$. It is evident that the theoretical and experimental curves follow similar trends on the same vertical scale, although the specific features of $\mathrm{Im}(\chi_0^{M})$ are different from those of $\mathrm{Im}(\chi_0^{\mathrm{expt.}})$ in the π-plasmon region. An improved model to link the graphene and graphite susceptibilities is proposed here, where the interlayer potential v_{3D} is replaced by $v_{3D}^{d^*}(d^*) = v_{\mathbf{00}}(d^*) \frac{\sinh[q(d-d^*)]}{\cosh[q(d-d^*)]-\cos[q_z(d-d^*)]}$, which depends on the effective "thickness" d^* of a graphene layer in graphite, from the point of view of the electron-electron interaction. The value of d^* changes with the total momentum $\mathbf{q}_{\mathrm{tot}} = (\mathbf{q}, q_z)$, ranging from $d^* = 0$ for $q_{\mathrm{tot}} \to 0$ to $d^* = d$ for $q_{\mathrm{tot}} \to \infty$. Amazingly, Figs. 3(b), 3(d), and 3(f) show that the theoretical susceptibility of graphite, calculated with this renormalized interaction as $\chi_{3D}^{M} = \frac{\chi_0^{M}}{1-v_{3D}^{d^*}\chi_0^{M}}$, is in excellent agreement with the measurements performed in [10], where d^* takes values from 3.10 to 3.27 Å for $0.212 < q < 0.563$ Å^{-1} and $q_z < 0.3$ Å^{-1}.

The dynamic properties of the effective fine-structure constant are dictated by the macroscopic inverse permittivity $(\epsilon^{M})^{-1}$, whose (minus) imaginary and real parts are reported in Figs. 4(a) [Fig. S6(a)] and 4(c) [Fig. S6(b)], respectively, with the π and σ-π structures being clearly outlined. Of particular importance is the static limiting behavior of $(\epsilon^{M})^{-1}$, or the $q \to 0$ and $\omega \to 0$ features of $\mathrm{Re}(\epsilon^{M})^{-1}$, which are explored with the outputs of datasets (ii) and (iii) yielding the lowest-q value $1/\epsilon_s = 0.054$ [Fig. 4(e)].

The main difference between the approach presented here and the derivation of [8,10] lies in the treatment of the $v\chi$ operator in ϵ^{-1}, whose macroscopic average $(v\chi)_{\mathbf{00}}$ is compared to the 2D approximated form $v_{2D}\chi_{2D}^{M}$ in Figs. 4(b) and 4(d), with the real and imaginary parts of the two quantities being normalized to the same height.

Apart from the above-discussed shift in q, $(v\chi)_{\mathbf{00}}$ and $v_{2D}\chi_{2D}^{M}$ have almost identical profiles, while the peak-to-peak ratios of their real (r_{2D}^{3D}) and imaginary (i_{2D}^{3D}) parts decrease with increasing q, similarly to $\frac{v_{\mathbf{00}}(L)}{v_{2D}L}$ [Fig. 4(f)]. This produces major errors in the estimation of α_g^*, obtained in [8,10] using

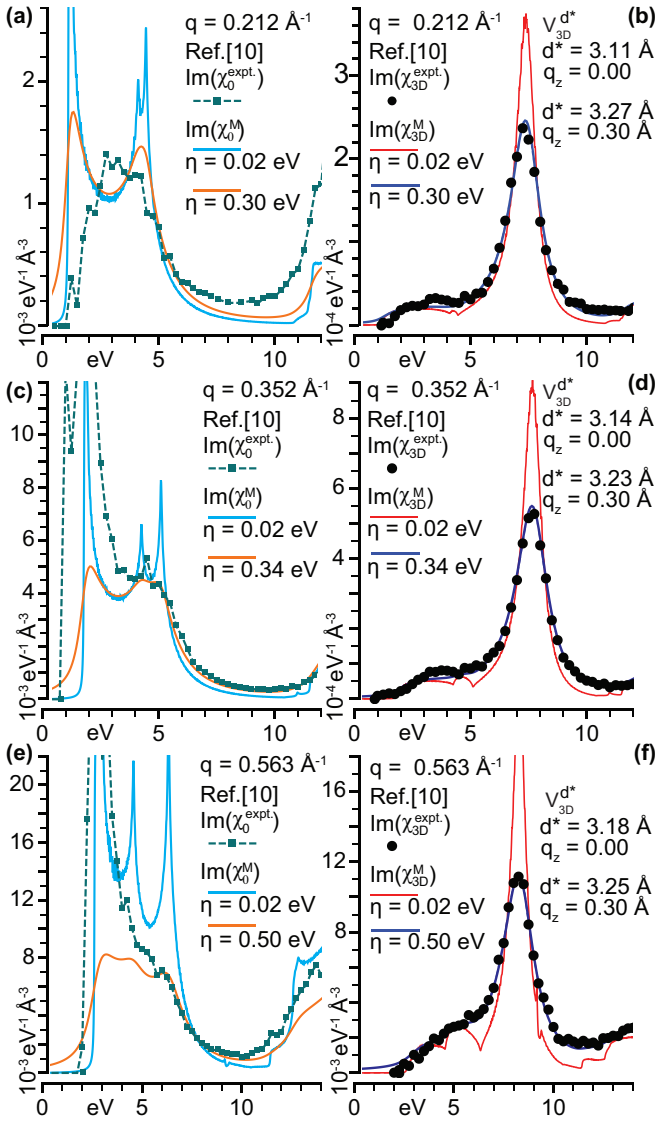

FIG. 3. Experimentally derived unperturbed susceptibility of graphene $\mathrm{Im}(\chi_0^{\mathrm{expt.}})$ and measured susceptibility of graphite $\mathrm{Im}(\chi_{3D}^{\mathrm{expt.}})$ taken from [10] in comparison with their theoretical counterparts $\mathrm{Im}(\chi_0^M)$ and $\mathrm{Im}(\chi_{3D}^M)$.

$(\alpha_g^*)_{\mathrm{expt.}} = \alpha_g(1 + v_{2D}\chi_{2D}^{\mathrm{expt.}})$, with the $\chi_{2D}^{\mathrm{expt.}}$ spectra of Fig. 2, which have been shown to have a close shape and intensity with the theoretical functions χ^M. On these bases, the following correction is proposed: $(\alpha_g^*)^{\mathrm{c}}_{\mathrm{expt.}} = \alpha_g(1 + r_{2D}^{3D} v_{2D}\chi_{2D}^{\mathrm{expt.}})$, being suitable for the $\omega \to 0$ limit with α_g^* becoming a real quantity [Figs. 4(b) and 4(d)]. The static value of α_g ranges from the LDA estimate of $\alpha_g^{\mathrm{LDA}} \sim 2.64$, equivalent to $v_F \sim 0.83 \times 10^6$ m/s [15], to the GW value of $\alpha_g^{\mathrm{GW}} \sim 1.95$, corresponding to $v_F \sim 1.12 \times 10^6$ m/s [13], or it may be taken to be ~ 2.20 as in [8,10,12], with $v_F \sim 1.0 \times 10^6$ m/s. In either case, the theoretical predictions of α_g^* are consistent with the corrected data $(\alpha_g^*)^{\mathrm{c}}_{\mathrm{expt.}}$ [Fig. 4(g)], within a percentage error of 5%–7%. In addition, a value of $\alpha_g^{\mathrm{LDA}}/\epsilon_s \sim 0.14$ is obtained at $q \sim 0.008$ Å^{-1}, in close agreement with [8].

In conclusion the strength of the electromagnetic interaction between charge carriers in graphene has been estimated by TDDFT [Eqs. (1) and (2)], using a truncated Coulomb potential

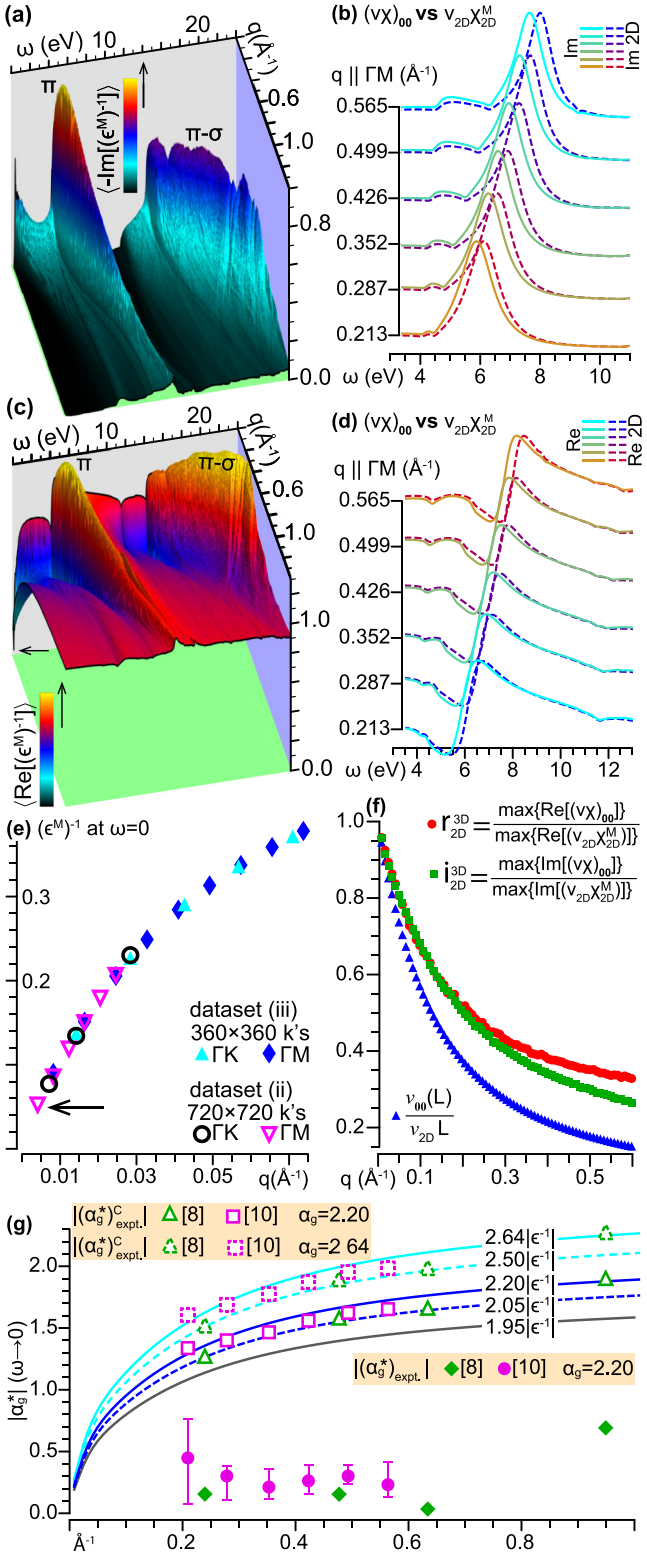

FIG. 4. (a),(c) $(\epsilon^M)^{-1}$ vs $\omega < 25$ eV and $q < 1.5$ Å^{-1}, with the **q** orientation averaged between ΓK and ΓM; (b),(d) $(v\chi)_{\mathbf{00}}$ and $v_{2D}\chi_{2D}^M$ vs $\omega < 13$ eV at fixed **q** values along ΓM that match the experimental in-plane momenta of [10]; (e) $(\epsilon^M)^{-1}$ vs $q < 0.1$ Å^{-1} at $\omega \to 0$, with the datasets (ii) and (iii); (f) peak-to-peak ratios r_{2D}^{3D}, i_{2D}^{3D} of the real and imaginary parts of $(v\chi)_{\mathbf{00}}$ and $v_{2D}\chi_{2D}^M$ vs $\frac{v_{\mathbf{00}}(L)}{v_{2D}L}$. (g) Dressed fine-structure constant α_g^* at $\omega \to 0$ in comparison with the experimentally derived data $(\alpha_g^*)_{\mathrm{expt.}}$ of [8,10], and the corrected data $(\alpha_g^*)^{\mathrm{c}}_{\mathrm{expt.}}$ with the r_{2D}^{3D} points of (f).

$[v_{\mathbf{GG}'}(L)]$ to describe the bare interaction between excited electrons. The calculations have been proved to accurately reproduce the measurements of [8,10], suggesting a calibration method to estimate α_g^*, based on the comparison of the density-density response function χ^M, obtained with $v_{\mathbf{GG}'}(L)$, and its 2D approximated form χ^M_{2D}, derived from $\delta_{\mathbf{GG}'} v_{2D} L$. The static limiting value of α_g^* has turned out to be suitable for perturbation expansion treatments of the many-body features of the band electrons in graphene. This result may have an impact in defining the transport properties of novel materials with a Dirac-cone structure, such as topological insulators, Weyl semimetals, or iron-based thin films.

A.S. acknowledges the computing facilities provided by the CINECA Consortium, within the INF16_npqcd project, under the CINECA-INFN agreement. S.B. acknowledges the financial support of the EU H2020 program under grant agreement AMD-696656-4 Graphene Core 1.

[1] K. S. Novoselov, A. K. Geim, S. V. Morozov, D. Jiang, Y. Zhang, S. V. Dubonos, I. V. Grigorieva, and A. A. Firsov, Electric field effect in atomically thin carbon films, Science **306**, 666 (2004).

[2] A. K. Geim and K. S. Novoselov, The rise of graphene, Nat. Mater. **6**, 183 (2007).

[3] A. H. Castro Neto, F. Guinea, N. M. R. Peres, K. S. Novoselov, and A. K. Geim, The electronic properties of graphene, Rev. Mod. Phys. **81**, 109 (2009).

[4] W. Ren and H.-M. Cheng, The global growth of graphene, Nat. Nanotech. **9**, 726 (2014); J. Liu, Charging graphene for energy, *ibid.* **9**, 739 (2014); K. Kostarelos and K. S. Novoselov, Graphene devices for life, *ibid.* **9**, 744 (2014); G. Fiori, F. Bonaccorso, G. Iannaccone, T. Palacios, D. Neumaier, A. Seabaugh, K. S. Banerjee, and L. Colombo, Electronics based on two-dimensional materials, *ibid.* **9**, 768 (2014); M. Dragoman, D. Neculoiu, A.-C. Bunea, G. Deligeorgis, M. Aldrigo, D. Vasilache, A. Dinescu, G. Konstantinidis, D. Mencarelli, L. Pierantoni, and M. Modreanu, A tunable microwave slot antenna based on graphene, Appl. Phys. Lett. **106**, 153101 (2015).

[5] P. R. Wallace, The band theory of graphite, Phys. Rev. **71**, 622 (1947).

[6] S. Das Sarma, S. Adam, E. H. Hwang, and E. Rossi, Electronic transport in two-dimensional graphene, Rev. Mod. Phys. **83**, 407 (2011).

[7] C. Jang, S. Adam, J.-H. Chen, E. D. Williams, S. Das Sarma, and M. S. Fuhrer, Tuning the Effective Fine Structure Constant in Graphene: Opposing Effects of Dielectric Screening on Short- and Long-Range Potential Scattering, Phys. Rev. Lett. **101**, 146805 (2008).

[8] J. P. Reed, B. Uchoa, Y. I. Joe, Y. Gan, D. Casa, E. Fradkin, and P. Abbamonte, The effective fine-structure constant of freestanding graphene measured in graphite, Science **330**, 805 (2010).

[9] E. Barnes, E. H. Hwang, R. E. Throckmorton, and S. Das Sarma, Effective field theory, three-loop perturbative expansion, and their experimental implications in graphene many-body effects, Phys. Rev. B **89**, 235431 (2014).

[10] Y. Gan, G. A. de la Peña, A. Kogar, B. Uchoa, D. Casa, T. Gog, E. Fradkin, and P. Abbamonte, Reexamination of the effective fine-structure constant of graphene as measured in graphite, Phys. Rev. B **93**, 195150 (2016).

[11] D. A. Bandurin, I. Torre, R. K. Kumar, M. Ben Shalom, A. Tomadin, A. Principi, G. H. Auton, E. Khestanova, K. S. Novoselov, I. V. Grigorieva, L. A. Ponomarenko, A. K. Geim, and M. Polini, Negative local resistance caused by viscous electron backflow in graphene, Science **351**, 1055 (2016); H. Zheng, Y. Gan, P. Abbamonte, and L. K. Wagner, Importance of σ Bonding Electrons for the Accurate Description of Electron Correlation in Graphene, Phys. Rev. Lett. **119**, 166402 (2017).

[12] T. Stauber, P. Parida, M. Trushin, M. V. Ulybyshev, D. L. Boyda, and J. Schliemann, Interacting Electrons in Graphene: Fermi Velocity Renormalization and Optical Response, Phys. Rev. Lett. **118**, 266801 (2017).

[13] P. E. Trevisanutto, C. Giorgetti, L. Reining, M. Ladisa, and V. Olevano, *Ab Initio* GW Many-Body Effects in Graphene, Phys. Rev. Lett. **101**, 226405 (2008).

[14] D. C. Elias, R. V. Gorbachev, A. S. Mayorov, S. V. Morozov, A. A. Zhukov, P. Blake, L. A. Ponomarenko, I. V. Grigorieva, K. S. Novoselov, F. Guinea, and A. K. Geim, Dirac cones reshaped by interaction effects in suspended graphene, Nat. Phys. **7**, 701 (2011).

[15] C. Hwang, D. A. Siegel, S.-K. Mo, W. Regan, A. Ismach, Y. Zhang, A. Zettl, and A. Lanzara, Fermi velocity engineering in graphene by substrate modification, Sci. Rep. **2**, 590 (2012).

[16] A. Sindona, F. Plastina, A. Cupolillo, C. Giallombardo, G. Falcone, and L. Papagno, Many body shake up in X-ray photoemission from bundles of lithium-intercalated single-walled carbon nanotubes, Surf. Sci. **601**, 2805 (2007).

[17] M. Petersilka, U. J. Gossmann, and E. K. U. Gross, Excitation Energies from Time-Dependent Density-Functional Theory, Phys. Rev. Lett. **76**, 1212 (1996).

[18] F. Aryasetiawan and O. Gunnarsson, The GW method, Rep. Prog. Phys. **61**, 237 (1998).

[19] G. Onida, L. Reining, and A. Rubio, Electronic excitations: Density-functional versus many-body Green's-function approaches, Rev. Mod. Phys. **74**, 601 (2002).

[20] V. Despoja, K. Dekanić, M. Šunjić, and L. Marušić, *Ab initio* study of energy loss and wake potential in the vicinity of a graphene monolayer, Phys. Rev. B **86**, 165419 (2012).

[21] V. Despoja, D. Novko, K. Dekanić, M. Šunjić, and L. Marušić, Two-dimensional and π plasmon spectra in pristine and doped graphene, Phys. Rev. B **87**, 075447 (2013).

[22] D. Novko, V. Despoja, and M. Šunjić, Changing character of electronic transitions in graphene: From single-particle excitations to plasmons, Phys. Rev. B **91**, 195407 (2015).

[23] M. Pisarra, A. Sindona, M. Gravina, V. M. Silkin, and J. M. Pitarke, Dielectric screening and plasmon resonances in bilayer graphene, Phys. Rev. B **93**, 035440 (2016).

[24] C. Vacacela Gomez, M. Pisarra, M. Gravina, J. M. Pitarke, and A. Sindona, Plasmon Modes of Graphene Nanoribbons with Periodic Planar Arrangements, Phys. Rev. Lett. **117**, 116801 (2016).

[25] C. Vacacela Gomez, M. Pisarra, M. Gravina, P. Riccardi, and A. Sindona, Plasmon properties and hybridization effects in silicene, Phys. Rev. B **95**, 085419 (2017).

[26] A. L. Fetter, Electrodynamics of a layered electron gas. II. Periodic array, Ann. Phys. (NY) **88**, 1 (1974).

[27] V. N. Kotov, B. Uchoa, V. M. Pereira, F. Guinea, and A. H. Castro Neto, Electron-electron interactions in graphene: Current status and perspectives, Rev. Mod. Phys. **84**, 1067 (2012).

[28] S. Yuan, R. Roldán, and M. I. Katsnelson, Excitation spectrum and high-energy plasmons in single-layer and multilayer graphene, Phys. Rev. B **84**, 035439 (2011); M. Pisarra, P. Riccardi, A. Cupolillo, A. Sindona, L. S. Caputi, Studies of electron emission in the interaction of electrons with graphene on Ni(111) surface, Nanosci. Nanotechnol. Lett. **4**, 1100 (2012); A. Sindona, S. A. Rudi, S. Maletta, R. A. Baragiola, G. Falcone, and P. Riccardi, Auger electron emission from metals induced by low energy ion bombardment: Effect of the band structure and Fermi edge singularity, Surf. Sci. **601**, 1205 (2007); P. Riccardi, A. Sindona, P. Barone, A. Bonanno, A. Oliva, and R. A. Baragiola, Bulk and surface plasmon excitation in the interaction of He^+ with Mg surfaces, Nucl. Instrum. Methods Phys. Res., Sect. B **212**, 339 (2003).

[29] X. Gonze, B. Amadon, P.-M. Anglade, J.-M. Beuken, F. Bottin, P. Boulanger, F. Bruneval, D. Caliste, R. Caracas, M. Cote *et al.*, ABINIT: First-principles approach to material and nanosystem properties, Comput. Phys. Commun. **180**, 2582 (2009).

[30] J. P. Perdew and A. Zunger, Self-interaction correction to density-functional approximations for many-electron systems, Phys. Rev. B **23**, 5048 (1981).

[31] N. Troullier and J. L. Martins, Efficient pseudopotentials for plane-wave calculations, Phys. Rev. B **43**, 1993 (1991).

[32] See Supplemental Material at http://link.aps.org/supplemental/10.1103/PhysRevB.96.201408 for (I) DFT computations of the ground-state properties and Fermi velocity of graphene with the parameters of datasets (i)-(iii), introduced in the main text and (II) TDDFT computations of the susceptibility and permittivity responses of graphene in comparison with some noteworthy experiments [10,41,42].

[33] P. Hohenberg and W. Kohn, Inhomogeneous electron gas, Phys. Rev. **136**, B864 (1964).

[34] W. Kohn and L. J. Sham, Self-consistent equations including exchange and correlation effects, Phys. Rev. **140**, A1133 (1965).

[35] H. J. Monkhorst and J. D. Pack, Special points for Brillouin-zone integrations, Phys. Rev. B **13**, 5188 (1976).

[36] M. Pisarra, A. Sindona, P. Riccardi, V. M. Silkin, and J. M. Pitarke, Acoustic plasmons in extrinsic free-standing graphene, New J. Phys. **16**, 083003 (2014); M. Pisarra, P. Riccardi, A. Sindona, A. Cupolillo, N. Ligato, C. Giallombardo, and L. Caputi, Probing graphene interfaces with secondary electrons, Carbon **77**, 796 (2014); A. Cupolillo, M. Pisarra, A. Sindona, M. Commisso, and P. Riccardi, Electron excitation in the interaction of slow ions and electrons with metals and monolayer graphite on Ni(111) surfaces, Vacuum **84**, 1029 (2010); M. Commisso, A. Bonanno, A. Oliva, M. Camarca, F. Xu, P. Riccardi, and R. A. Baragiola, Plasmon excitation and electron promotion in the interaction of slow Na^+ ions with Al surfaces, Nucl. Instrum. Methods Phys. Res., Sect. B **230**, 438 (2005).

[37] S. L. Adler, Quantum theory of the dielectric constant in real solids, Phys. Rev. **126**, 413 (1962).

[38] N. Wiser, Dielectric constant with local field effects included, Phys. Rev. **129**, 62 (1963).

[39] C. Kramberger, R. Hambach, C. Giorgetti, M. H. Rümmeli, M. Knupfer, J. Fink, B. Büchner, L. Reining, E. Einarsson, S. Maruyama, F. Sottile, K. Hannewald, V. Olevano, A. G. Marinopoulos, and T. Pichler, Linear Plasmon Dispersion in Single-Wall Carbon Nanotubes and the Collective Excitation Spectrum of Graphene, Phys. Rev. Lett. **100**, 196803 (2008).

[40] K. W. K. Shung, Dielectric function and plasmon structure of stage-1 intercalated graphite, Phys. Rev. B **34**, 979 (1986).

[41] S. C. Liou, C.-S. Shie, C. H. Chen, R. Breitwieser, W. W. Pai, G. Y. Guo, and M.-W. Chu, π-plasmon dispersion in free-standing graphene by momentum-resolved electron energy-loss spectroscopy, Phys. Rev. B **91**, 045418 (2015).

[42] T. Eberlein, U. Bangert, R. R. Nair, R. Jones, M. Gass, A. L. Bleloch, K. S. Novoselov, A. Geim, and P. R. Briddon, Plasmon spectroscopy of free-standing graphene films, Phys. Rev. B **77**, 233406 (2008).